American Mineralogist, Volume 101, pages 1072–1083, 2016

Petrographic investigation of smithing slag of the Hellenistic to Byzantine city of Sagalassos (SW-Turkey)

Kim Eekelers[1,*], Patrick Degryse[1], and Philippe Muchez[1]

[1]Earth and Environmental Science, Katholieke Universiteit Leuven, Celestijnenlaan 200E, 3001 Heverlee, Belgium

Abstract

The frequent occurrence of iron slag in excavation layers of the Hellenistic to Byzantine city of Sagalassos (SW Turkey), indicates continuous iron working from the 1st to 7th century A.D. The slag samples are identified as smithing hearth bottoms and are found in dump fills, building foundations, and road constructions. Although several smelting sites are present in the 1800 km^2 large territory of the city, the chemical signature of the smelting slag does not correspond to the characteristics of the smithing slag found in the city itself. The smithing slag does offer insight in the smithing techniques applied, which in turn provides information about the objects produced and production chain or "chaîne opératoire" followed for iron production in Sagalassos. Textural and mineralogical analyses reveal two main smithing techniques that were applied throughout the 1st to 7th century A.D. The most commonly applied smithing technique is used for the production of simple bulk materials, like hammers or anvils. Microscopic textures in the slag show mainly mechanical deformation at relatively high temperatures. The second, more sophisticated smithing technique shows the blacksmith treated the iron at different temperatures. The presence of high-lime contents indicates the use of a flux and/or a protective agent against oxidation. This technique was applied to make more complex objects or objects with cutting edges. Based on the reconstruction of the smithing techniques, the iron production of Sagalassos produced mainly everyday bulk material. The current study demonstrates the importance of using the mineralogy of smithing slag in reconstructing the technological evolution of iron production. Microtextural and mineralogical studies and comparison with modern smithing techniques offer greater insight in the complex world of Roman blacksmithing.

Keywords: Iron slag, archaeometallurgy, smithing, mineralogy, textural analysis, optical microscopy, XRD analysis, Rietveld, ICP-OES

Introduction

The occurrence of metallurgical waste throughout the 1800 km^2 territory of Sagalassos, with several smaller settlements and the monumental Hellenistic to Byzantine city of Sagalassos (SW Turkey) itself, indicates continuous iron working there (Fig. 1). The metallurgical waste found consists of smelting and smithing slag, hammer scale, bloom, and rejected ore. In Antiquity, iron objects were produced in a two step (sometimes three steps) process (Fig. 2). Iron ore, usually iron oxides or carbonates of sufficient high grade, were mined and prepared by removing the gangue material, reducing the size of the ore lumps and roasting the ore to lose volatiles, such as hydrogen and sulfur (Serneels and Perret 2003). During smelting by a direct reduction process, the iron oxides were reduced in solid state by heating the ore with charcoal in a closed furnace at a temperature between 1000–1200 °C (Cleere 1971; Serneels and Perret 2003; Charlton et al. 2013). The carbon monoxide produced in the furnace causes the iron ore to be reduced to its metallic state, resulting in almost pure iron that is called a bloom (Serneels and Perret 2003). Other substances, mainly silica, alumina, lime, and unreduced iron oxides form a liquid phase, which separates from the bloom and flows away, resulting in an iron smelting slag (Serneels and Perret 2003). Since this process is not efficient, the bloom still has slag inclusions and the slag contains much iron. In a next step the bloom will be further refined during the primary smithing process and shaped into currency bars. These bars are then used in a secondary smithing process, where the iron is shaped by plastic deformation (repeatedly heating and hammering) by the blacksmith to make the final object (Serneels and Perret 2003). Waste associated with this last step forms smithing slag, which is an accumulation of fused residual material characterized by a plano-convex shape (Serneels and Perret 2003).

In the monumental city of Sagalassos, smithing slag are found in several excavation layers dating from the 1st to 7th century A.D. (Kellens et al. 2003). Most of the slag are related to destruction layers or are used in fills or to level roads. Some are, however, found in occupation layers associated with hammer scales indicating the presence of smithing workshops (Kellens et al. 2003). Slag are not limited to the Antique city, but are found throughout the territory. In the Bey Dağlari Massif, 5 km east of the city, smelting slag are present in two sites (Tekeli Tepe and Dereköy). Moreover, geophysical research at Tekeli Tepe revealed the presence of furnaces. Ceramics tentatively date the slag to the 6th–7th century A.D. Also in the Hellenistic settlement

* E-mail: kim.eekelers@arts.kuleuven.be

0003-004X/16/0005–1072$05.00/DOI: http://dx.doi.org/10.2138/am-2016-5390

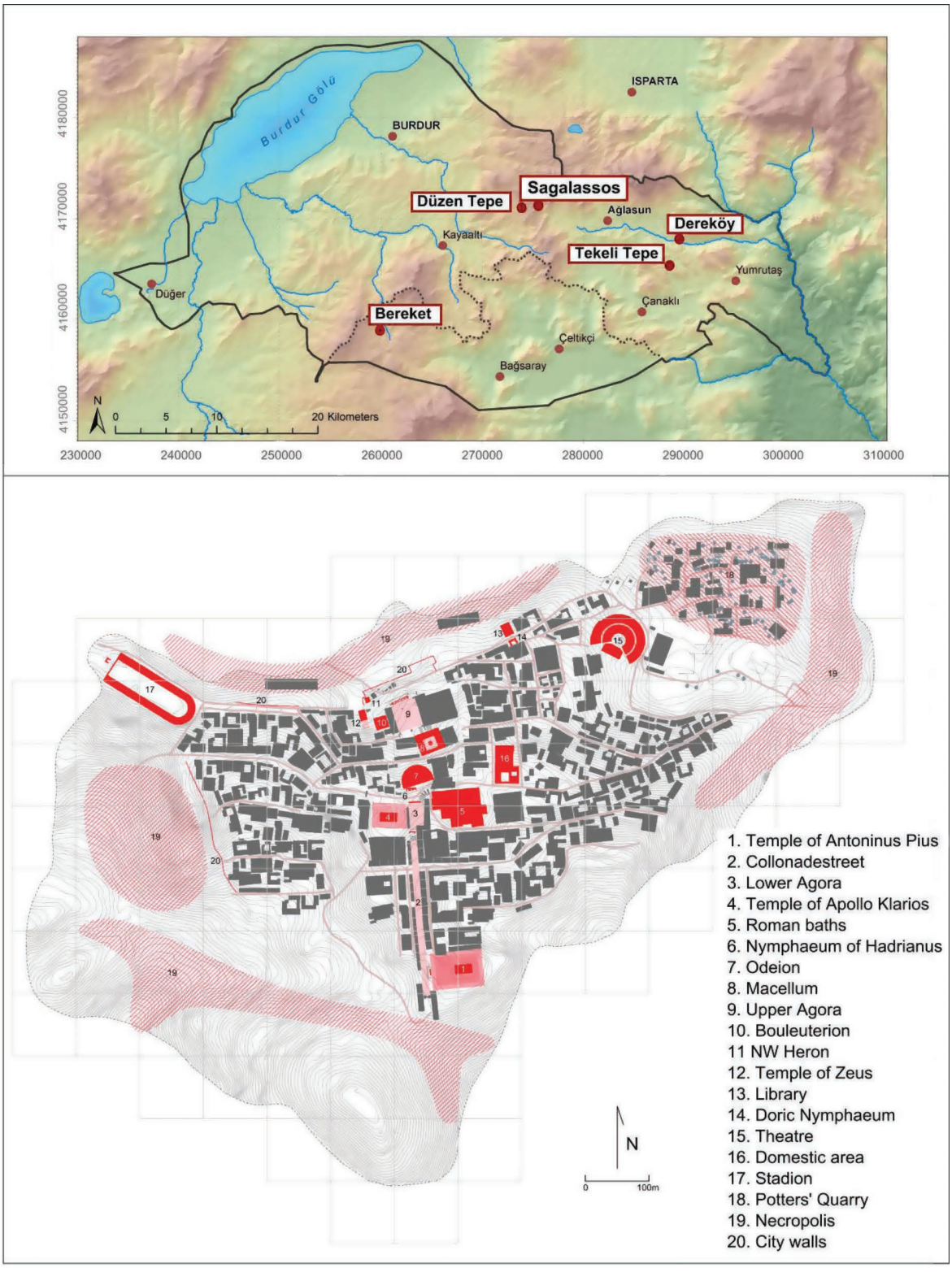

FIGURE 1. (**top**) Outline of the Sagalassos territory during Roman times. The different sites were metallurgical waste is found are indicated on the map. (**bottom**) The monumental city of Sagalassos. Smithing slag used for this study are found at (1) Temple of Antoninus Pius, (9) Upper Agora, (10) Bouleuterion, (13) Library, (14) Doric Nymphaeum, (16) Domestic area, (18) Potters' Quarter, (19) City survey in the Necropolis.

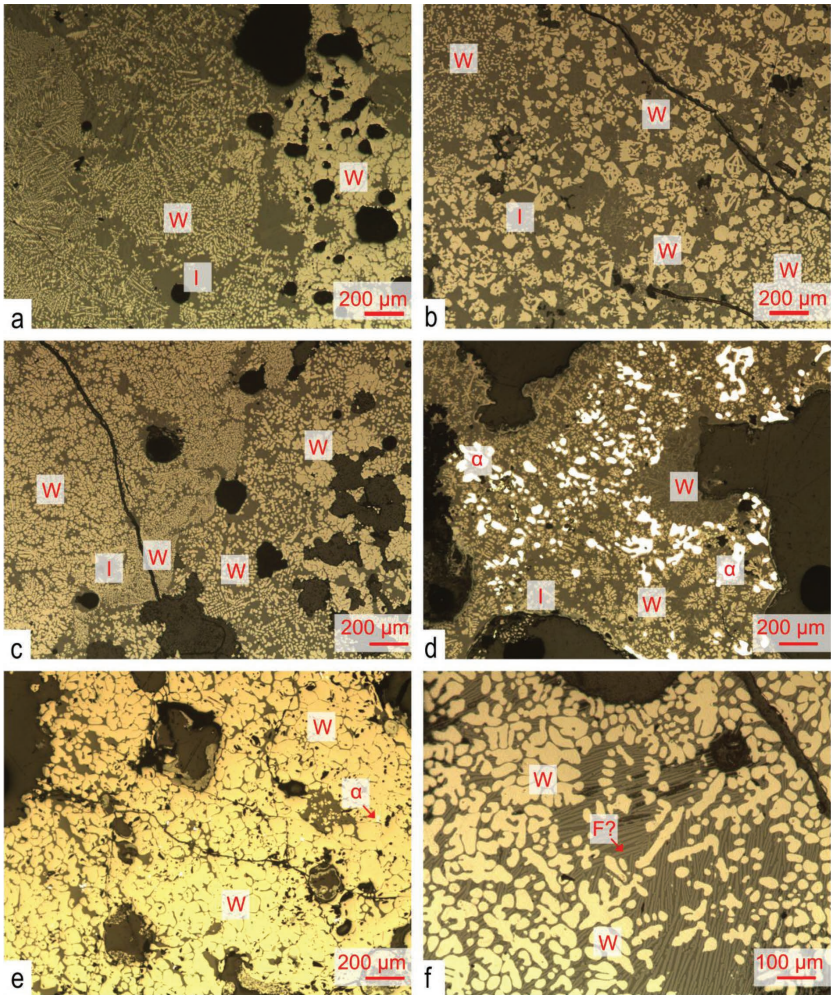

Figure 2. (**a**) Transition of skeletal to closely packed wüstite (approaching hammer scale texture) in group A. (**b**) Hopper-shaped wüstite in group A. (**c**) Transition of closely spaced wüstite to a patch texture in group A. (**d**) Ferrite loss (white mineral) in group A. (**e**) Hammer scale texture with small loss of ferrite (white dots) in group B. (**f**) Feather-shaped laths between little branched wüstite in group B. W = wüstite, I = interstitial glass, F? = feathershaped laths and α = α-iron.

of Düzen Tepe (1.8 km SW of the monumental city, 5th–2nd century B.C.; Vyncke 2013) and the settlement of Bereket (25 km SW of the monumental city, age unknown) smelting sites are located. Conversely, though smithing slag are commonly found, finds of smelting slag in Sagalassos are very rare. One tap slag was found in a street sounding and is likely related to the leveling of the road. It was dated to the first century A.D. (Kellens et al. 2003). Another tap slag, dated to the second century A.D., was used to fill a ditch associated with the construction of the Roman Library. One furnace-cooled smelting slag was found at the Upper Agora in association with a large number of metal objects (3rd century A.D.).

Previous studies on the iron slag of the Sagalassos territory mainly focused on provenancing and linking the slag and iron objects to their potential ore source. Several mineralizations are located in the territory of Sagalassos. Chemical and mineralogical analysis on slag from the monumental city (1st–7th century A.D.) and from the Bey Dağlari massif (6th–7th century A.D.) show a distinct difference in the type of ore source used (Degryse et al. 2003a). While the slag of the city carried the chemical signature of a typical Roman slag with elevated iron and silica values, the slag from Bey Dağlari showed an elevated titanium, vanadium, and zirconium content (Degryse et al. 2003a). At Dereköy, slag and furnace material were found in association with a spinel placer deposit. The ore source used for the Sagalassos iron, however, remains unclear. Although a hematite mineralization occurs in the immediate proximity of the city, it is low grade, which makes it unsuitable for iron production (Degryse et al. 2003a).

Pb- and Sr-isotopes have also been employed to assign iron artifacts and metallurgical waste to potential ore sources (Degryse et al. 2007, 2009). The Pb-content of the Hellenistic objects from Düzen Tepe is too low to perform Pb-isotope analysis. The objects, however, are found in association with a magnetite placer deposit, which is a likely candidate as the ore used at this site (Vyncke 2013). Early Roman objects in turn seem to relate to the hematite deposit located in the proximity of the city. Due to

the disseminated nature of the ore, it is possible that higher grade ore then those measured in the 2003 study, were employed in Antiquity (Degryse et al. 2007). A potential ore source for Late Roman artifacts lies in Camoluk. This Fe-Mn mineralization is located just south of the territory and was possibly imported into the territory. Early Byzantine artifacts and waste material likely originate from the spinel placer deposit at Dereköy (Degryse et al. 2007, 2009).

Although considerable research has been devoted to provenancing the iron objects and ores, less attention has been paid to integrated archaeometric research on the slag and their meaning for Sagalassos. One of the major research topics of the interdisciplinary Sagalassos project is the reconstruction of the economy, social organization, and ecology of the site and its territory. From a ceramic perspective, macro- and microscopic descriptions has been completed to deduce the applied technology (Degryse et al. 2003b).

The iron slag found at several locations in the city and territory have similar potential to estimate the importance of iron production in the Sagalassos territory. This paper concentrates on the smithing slag found in the monumental city. Most archaeometallurgical research concentrates on smelting technology. Less attention goes to smithing slag, which is probably due to the complex nature of this waste material. The composition of smelting slag depends on the furnace operation (design, air supply mechanism), raw material used (ore, charcoal, furnace lining) and potential use of a flux (Cleere 1976). When studying smithing slag, extra variables are to be taken into account. The morphology, composition, and microtextures of smithing slag depend on the bloom used (which in turns depends on the smelting recipe) and the complexity of the object that is produced. These two parameters influence the type of hearth used, the hearth temperature and the actions of the blacksmith (simple heating, hammering, welding, cementation) (Crew 1996; Serneels and Perret 2003; Berranger and Fluzin 2007; Le Carlier et al. 2007; Young 2012) (e.g., if the object is large, welding may be necessary). In that case, the blacksmith will use a flux to remove the oxidation layer that appears when the iron is taken out of the hearth (Crew 1996; Le Carlier et al. 2007; Rehren and Pernicka 2008). Importantly, the experience of the blacksmith is a variable that is difficult to account for (Crew 1991). All these factors result in a slag composition that can be further removed from equilibrium conditions than for smelting slag (Rehren and Pernicka 2008). Conversely, smithing slag offer the opportunity to study the intermediate stages of the various operations carried out at an iron workshop.

Serneels and Perret (2003) related the macroscopic variability in morphology of the iron slag to the smithy process. They distinguish between three textures. A scorie grise dense (SGD) is dominated by fayalite with a variable amount of iron oxides and small amount of interstitial glass and is related to hot oxidation during smithing with a small input of silica. The scorie argillo-sableuse (SAS) is rich in silica and has a low-iron content. The silica presence indicates the use of a flux that is related to welding or minimizing oxidation in the finishing phase. The scorie ferreuse rouillée (SFR) is characterized by the presence of metallic iron, iron oxides, and -hydroxides. This type of slag is related to high-temperature operations or use of a poorly compacted raw material. Le Carlier et al. (2007) investigated slag at microscopic scale and described different mineralogical phases. They reconstructed the "chaîne opératoire" of the iron production in Puy-de-Grâce (Perpezac-Le-Noir, France) based on a microscopic analysis of the smithing slag. Berranger and Fluzin (2007) used information gained from smithing slag to reconstruct the social organization of workshops at Entremont (Aix-en-Provence, France). Smithing slag are made up of different mineralogical associations, depending on the different operations that took place. Hammer scales in the slag are hemispheric textures consisting of iron oxides and metallic iron that are knocked off during hammering. Sometimes this iron starts to melt and forms new phases in the hearth. Complex silicates may indicate the use of fluxes applied for welding or anti-oxidation. Sometimes also clay-sand-rich zones can be recognized. This material originates from fluxes and hearth lining, but did not melt in the hearth. The smithing slag of Sagalassos will be studied with petrography and chemistry to reconstruct the smithing technologies used in Roman times. Additionally, since most slag samples are dated based on associated ceramic chronology, change in smithing techniques through time can be checked.

Experimental methodology

Materials

One hundred and fifty-five slag samples were compositionally analyzed. Of these samples, 22 smithing heart bottoms (SHB) were used for mineralogical and petrographic analysis, selected based on find location, age, and morphology [using the classification of Serneels and Perret (2003)]. The SHB are found at different locations in the city and represent 20 yr of excavations (Table 1; Fig. 1). The waste material is dated to the Early to Late Roman period (25 B.C. to 450/75 A.D.) (Tables 1 and 2) based on associated diagnostic ceramic material of which a detailed chronology was drawn up throughout the years (Poblome 1999). Most of the samples are found as dump fill or were used for construction (roads, foundations, …). Some samples were collected during urban survey. Although more difficult to date, the survey slag were dated based on distribution maps and diagnostic sherds (Martens 2005).

Microscopy

Polished sections are made from the iron-rich parts of the slag. A Nikon Eclipse 50 POL with reflected light and total magnification of 500 was employed for light microscopy. Pictures were taken using a Leica DMLP microscope with Deltapix D200 CCD camera supported by Axionvision software.

X-ray diffraction (XRD)

Since the optical properties of iron, calcium, and aluminum silicates are similar and thus not readably distinguishable using regular light microscopy, XRD is used to complete a full mineralogical characterization of the slag. To verify whether the mineralogical composition of the slag is technology or age dependent, quantification is necessary. Minerals are 3D-ordered structures with characteristic periodicities along crystallographic axes. Incident X-rays are diffracted by these planes, forming the base of powder diffraction and allowing identification of minerals present in the slag (Klein and Dutrow 2008). To quantify the minerals, the Rietveld method using the Direct Convolution approach, was employed. This method determines the best fit between the measured and calculated diffraction pattern using a least-square refinement (Rietveld 1967). The calculated pattern is modeled by refining the crystal structure, the diffraction optic effects, instrumental factors and other specimen characteristics as strain and crystal size (Mertens 2009).

Samples are prepared by grinding and sieving them ≤250 μm. Next 2.7g of the sample and 0.3 g of an internal standard are mixed and micronized in a Mc-Crone Micronizing mill with 5 mL ethanol as grinding agent for 5 min. Zincite (ZnO) is chosen as internal standard following the procedure described by Środoń et al. (2001). After two days of drying, samples are disaggregated in a mortar and passed through a 250 μm sieve to ensure good mixing between the sample and the

Table 1. Sample list with location, age, and context of the selected slag

Sample	Location	Age	Period	Context
N311B	Nymphaeum	1st half 4th century A.D.	Late Imperial	Dumpfill
N396	Nymphaeum	1st half 2nd century A.D.	Mid Imperial	Dumpfill
N70E	Nymphaeum	1st half 4th century A.D.	Late Imperial	Dumpfill
N288	Nymphaeum	1st half 4th century A.D.	Late Imperial	Dumpfill
N118	Nymphaeum			Soil layer
N323	Nymphaeum	1st half 4th century A.D.	Late Imperial	Dumpfill
N533d	Nymphaeum	1st half 4th century A.D.	Late Imperial	Dumpfill
N195b	Nymphaeum	1st half 4th century A.D.	Late Imperial	Dumpfill
N311	Nymphaeum	1st half 4th century A.D.	Late Imperial	Dumpfill
N269b	Nymphaeum	1st half 4th century A.D.	Late Imperial	Dumpfill
CS022	City survey			Surface find
CS027	City survey		Early to Late Imperial	Surface find
CS097	City survey		Early to Mid Imperial	Surface find
CS264	City survey		Late Imperial to Early Byzantine	Surface find
WS1-008a	Sondage	2nd half 5th – 6th century A.D.	Early Byzantine	Test sounding in the east-west street west of the Lower Agora
DA2-177	Domestic area 2	2nd to 3rd century A.D.	Mid Imperial	Substratum and floor level in beaten earth, together with other production waste (mortar, stone, coarse ware, fragmented ceramics)
PQ35B	Potters' quarter			
91F	Potters' quarter			
UAN232	Upper Agora Nord			
AP181C	Antonius Pius	1st century A.D.	Early Imperial	Layer above ophiolitic bedrock
DT097	Doric Temple			
B263	Bouleuterion			
L475	Library	Late 1st – Early 2nd century A.D.	Early-Mid Imperial	
LW033	Library West			
LE600b	Library East	2nd half 4th century A.D.	Late Imperial	

standard and limit preferred orientation. Next the sample is transferred into the sample holder by back loading.

Samples are measured with a Phillips PW180 diffractometer with a Bragg/Brentano θ-2θ setup and Cu*K*α radiation at 45 kV and 30 mA. The scan ranges from 5 to 75° with a step size of 0.02 and 2 s per step. The software used for identification is EVA. Minerals are quantified with Rietveld refinement TOPAS Academic. The implementation code is refined as described by Baerlocher (1986).

During the XRD studies on the slag samples two problems with the quantification refinement were identified: the abundance of wüstite was underestimated, while the abundance of the amorphous phase were overestimated when compared to observations made from polished sections. To resolve the latter, the internal standard, zincite, was checked to be adequate for iron slag. If it was too soft, it would be ground to an amorphous phase in the preparation process. During the test, the sample was first micronized to 10 µm and afterward the zincite was added. After analysis, no significant difference was noted between the micronized zincite and the later added standard. Next the absorption of the Cu*K*α-radiation by the slag was tested by comparing it to Co*K*α radiation. After analysis, a significant difference in amorphous material and wüstite was observed. The use of a Co*K*α-tube causes electrical problems in the laboratory and was not a sustainable solution. The most acceptable method for analysis was to apply an empirical absorption coefficient to the data reduction implementation code. Although the estimates of wüstite abundance improved significantly, problems still occur in modeling the wüstite peak at 42° 2θ. Since wüstite belongs to the cubic crystal system, preferred orientation is limited. It was discovered that introducing wüstite with different crystallite sizes (one large to cover the broadness of the peak, one small to fill the height of the peak), a better quantification was achieved.

Table 2. General timeframe of Sagalassos (Waelkens 2002)

Byzantine (450/475–1453 A.D.)	Late (middle 11th century A.D. to 1453 A.D.)
	Middle (2nd half 7th century A.D. to middle 11th century A.D.)
	Early (565 A.D. to 1st half 7th century A.D.)
Roman/Imperial (25 B.C. – 450/75 A.D.)	Late (284 to 565 A.D.)
	Middle (2nd century A.D. to 3rd century A.D.)
	Early (25 B.C. to 1st century A.D.)
Hellenistic (333–25 B.C.)	Late (1st century B.C. to 25 B.C.)
	Middle (2nd century B.C. to early 1st century B.C.)
	Early (333 B.C. to 3rd century B.C.)

Compositional analysis

Samples were analyzed by inductively coupled plasma-optical emission spectrometry (ICP-OES). Elements were extracted using an adapted $LiBO_2$ fusion procedure. Samples were prepared by removing the outer oxidation rim. They were dried for 24 h at 60 °C. The samples were mechanically milled using a Phillipmill, which results in a grain size between 90 and 180 µm. A 250 mg aliquot of each sample was oxidized in ceramic boats for 2 h at 1000 °C. After cooling, 50 mg of sample was weighed, mixed with 1000 mg of $LiBO_2$, transferred into a graphite crucible and heated at 880 °C for 10 min. The viscous molten sample was dissolved into HCl (2.5 M) and stirred. After diluting the solution 10 times in HNO_3 (0.42 M), element intensities were measured using a Varian 720-ES instrument supplied with a double-pass glass cyclonic spray chamber, concentric glass sea spray nebulizer and "extended high solids" torch. An ionization buffer (1% $CsNO_3$ in 4% HNO_3) was added. Al, Ba, Ca, Co, Cr, Cu, Fe, K, Mg, Mn, Na, Ni, P, Si, Sr, Ti, V, Zn, and Zr are measured. Standard reference material (SRM) NIM-L, MRG-1, PRI-1, NBS 120b, BCS 175/2, probe 627-2, and NIST 610 are extracted and measured in a similar way to the samples to ensure matrix matching. Calibration curves were obtained from procedural blanks (2 per batch) and SRM's (Brems 2011). Data precision and accuracy was evaluated by analysis of replicate and certified reference materials (probe 627-2). Accuracy (Table 3), expressed as the deviation of the measured concentrations compared to the certified concentration, is lower than 10% for all elements. Precision (Table 4), expressed as the procentual standard deviations, is lower than 10% for all elements with the exception of Na_2O and SiO_2.

Results

Microtextures

Samples may be separated into two groups based on observed microtextures. Group A (Figs. 2a, 2b, 2c, and 2d; Table 5) shows layering in the crystal habit of wüstite. Wüstite is distinguished from magnetite, it is lighter and shows a yellowish gray color, while magnetite has a more brownish tint (Bachmann 1982; Deer et al. 2013). Wüstite habit varies from skeletal, to dendritic, to hopper shaped (Donaldson 1976) to more subhedral, compacted crystals. The matrix is amorphous or displays feather-shaped laths of silicate minerals. Ferrite is present as globules or shaped

Table 3. Accuracy of SRM probe 627–2 expressed as the deviation between the measured concentration compared to the certified concentration

	Al_2O_3	CaO	Fe_2O_3	MgO	MnO	SiO_2	TiO_2
%	0.52	0.81	1.59	2.00	0.84	2.70	8.22

Table 4. Precision of SRM probe 627–2 expressed as the percentual standard deviation

	Al_2O_3	BaO	CaO	Fe_2O_3	K_2O	MgO	MnO	Na_2O	SiO_2	TiO_2
St. dev.%	7.24	6.99	7.79	3.35	7.66	2.01	5.05	18.03	10.70	5.21

as a puzzle piece between larger dendrites. Group B (Figs. 2e and 2f; Table 5) is not stratified and wüstite shows little variation in crystal habit. This group is characterized by a large amount of small branched wüstite dendrites that are heavily compacted. Between the dendrites feather-shaped laths of iron and/or calcium silicates are visible. These are orientated or show a graphic pattern. In some patches, the crystal edges of the wüstite are no longer well defined as they form anhedral crystals. These patches are usually hemispherical (hammer scale). Occasionally a patch with more spaced dendrites and even skeletal wüstite is present. These textures are usually associated with pores. Ferrite appears as globules or fits between the dendrites of wüstite. Little amorphous material is recognized. Five samples deviate from the two main groups. PQ35 and DT97 (Figs. 3a and 3b; Table 5) are limitedly stratified and show a patched texture. Some patches of wüstite display a skeletal texture, while others are closely packed evolving to the typical hammer scale texture. Samples found at the Antonius Pius Temple (AP181c1-AP181c2) (Figs. 3c and 3d; Table 5), show a myrmekitic texture. The wüstite dendrites are closely packed. Sample N70 (Figs. 3e and 3f; Table 5) is characterized by its low wüstite content. It appears mostly as skeletal or irregular dendritic shapes. The sample distinguishes itself by large feather-shaped laths of silicates that are dominant in the matrix. Irregular ferrite is observed. Moreover, crystals with twinning structures are recognized.

Mineralogical composition

XRD results show a complex mixture of iron oxides (wüstite, magnetite, hematite), silicates (fayalite, forsterite, kirschsteinite, wollastonite), spinel (hercynite, ulvospinel), amorphous material and alteration products [goethite, lepidocrocite, akaganeite, gypsum (Serneels 1993)] (Table 5). The quantified results are placed in the groups obtained by texture analysis (cf. 3.1) to check whether the groups are also distinguishable based on mineralogy. These results are visualized in boxplots. Group A (Fig. 4; Table 6) has high values for calcite, akermanite, and amorphous material. Occasionally hercynite and bredigite are present (Table 6). Also the lepidocrocite content is elevated, but is not considered further since this is an alteration product (Serneels 1993). Group B (Fig. 4; Table 6) is characterized by high wüstite. It is also the only group where cohenite is present. Also akaganeite shows elevated values, but since this is a mineral associated with alteration, it is not treated further here (Serneels 1993). The Antonius Pius samples (Fig. 4; Table 6) are characterized by elevated magnetite, hematite, and quartz, while N70 (Fig. 4; Table 6) is dominated by the presence of forsterite and kirschsteinite. Samples PQ35 and DT97 are characterized by the presence of monticellite and have a high content in amorphous phases (Fig. 4).

Table 5. Classification of the slag samples in their respective groups based on microscopy and DFA and corresponding age

Age	Group A (T = 5)	Group B (T = 12)	Exceptions
Early Imperial	CS097	CS097, L475	AP181c
Mid Imperial	N396	DA2–177	
Late Imperial	N311b, N288	N323, N296b, CS264, LE600b	N070e, PQ035b
Unknown	N195	CS022, LW033, UAN232, B263, 91F	DT097

Chemical composition

The composition of the textural groups is presented in Figure 5 and Table 7. Group A is rich in CaO, P_2O_5, SiO_2, and Cu compared to group B and the deviating samples. It shows a large standard deviation for the CaO, Cu, Fe_2O_3, and SiO_2 content. Sample N70E has an elevated CaO, MgO, Na_2O, SiO_2, and TiO_2 content compared to the other groups. PQ35 and DT97 distinguish themselves by higher K_2O, MgO, Na_2O, and SiO_2 values relative to the other groups. The Antonius Pius samples stand out by their high Fe_2O_3 values. Group B shows average values compared to group A and the deviating samples. Only Fe_2O_3 is elevated. Samples belonging to group B, show also a large standard deviation for CaO, Fe_2O_3, and SiO_2.

Discussion

Group A: Temperature-dependent group

The observed layering in wüstite textures indicates the use of different smithing techniques at different temperatures during smithing. The skeletal shapes of wüstite represent rapid cooling of the fragment and possibly quenching (Serneels 1993; Bauvais 2007), evolving to more standard dendritic shapes still shows fast cooling, but without quenching. These forms most likely occur when the metal is taken out of the hearth and cools immediately to room temperature. Hopper shapes may be explained by a similar process (Serneels 1993; Bauvais 2007). The more compacted crystals of wüstite represent hammer scales, which are an indication for mechanical working of the material (Crew 1991; Bauvais 2007). By hammering the material, the outer oxidation layer is expelled, resulting in flat hammer scales (Crew 1991). Mineralogical, this group is characterized by the presence of a high calcite ($CaCO_3$) and akermanite [$Ca_2Mg(Si_2O_7)$] content. Akermanite is typically found in modern blast furnace slag and has a high-melting temperature (1454 °C). However, when iron is incorporated into the crystal structure its melting temperature is lowered to 775 °C. Bredigite [$Ca_7Mg(SiO_4)_4$] is stable between 725 and 1450 °C (Kiessling and Lange 1978). When it is cooled further, the mineral stays stable or transforms to larnite or shannonite. Hercynite ($FeAl_2O_4$), which is observed in one sample, is a high-temperature mineral. At atmospheric pressure its melting temperature exceeds 1000 °C. However, if cordierite [$(Mg,Fe)_2Al_3(AlSi_5O_{18})$] was present in the original iron bar, it would break down to hercynite and quartz (SiO_2) when cooled to 775–340 °C (Bowles et al. 2011). The elevated content of calcite in this group stands out. Calcium is used as a flux in the smelting process. It minimizes the loss of iron and makes the slag more fluid (Sim 1998). Another possible explanation for the presence of calcite in the slag, is the dissociation of wollastonite ($CaSiO_3$), which could have been present as slag in the trade bar, to calcite and quartz when cooling below 500 °C (Deer et al. 1978). Based on the mineralogy, it is inconclusive to deduce smithing tempera-

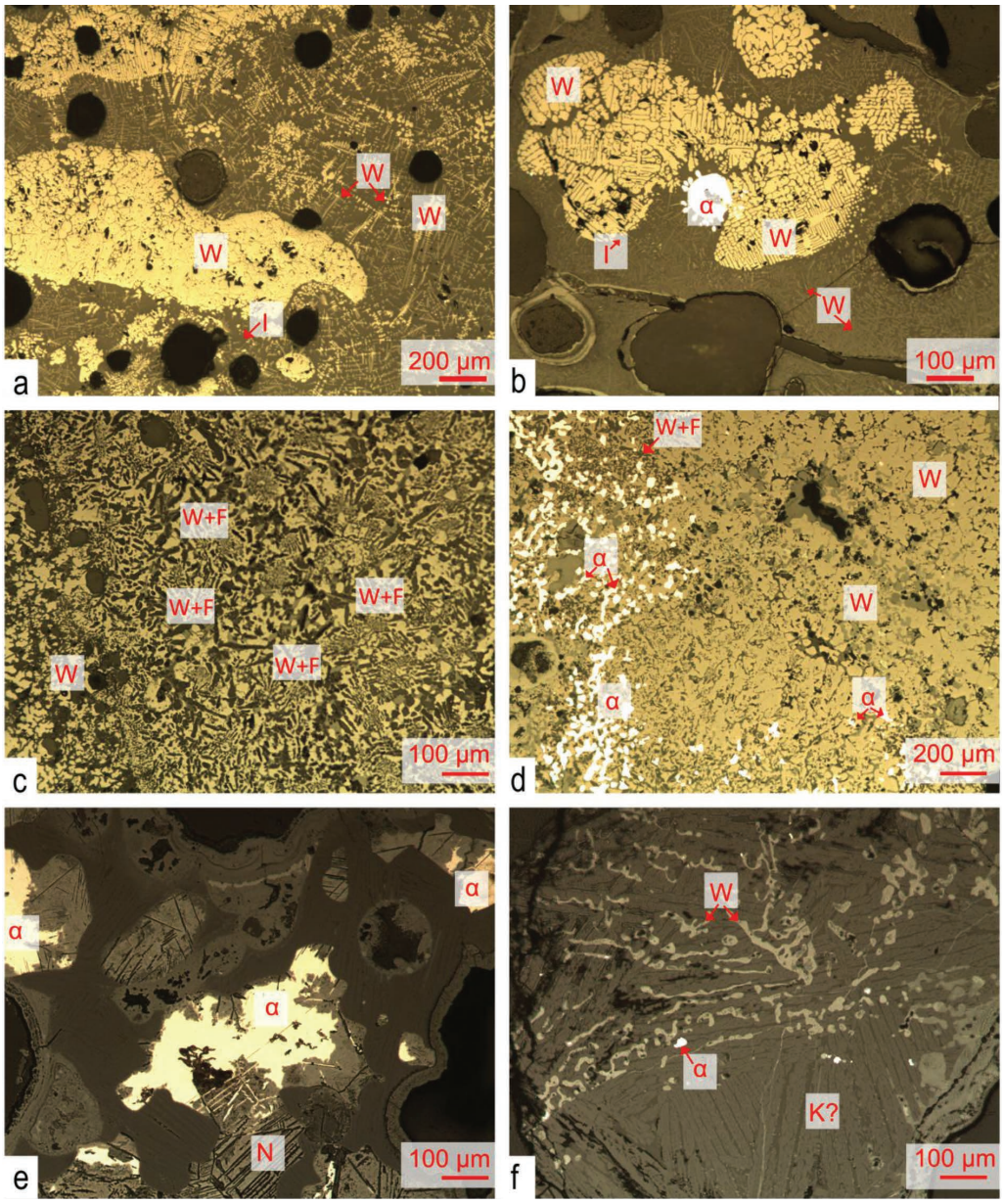

FIGURE 3. (**a**) Patched texture of wüstite in amorphous matrix in PQ35. (**b**) Patched texture of wüstite with globule of ferrite (white) in PQ35. (**c**) Myrmetic texture in wüsite in AP. (**d**) Closely packed dendrites with ferrite loss in AP. (**e**) Ferrite loss and mechanical twinning in iron oxide in N70. (**f**) Irregular wüstite dendrites and feather-shaped texture in matrix in N70. W = wüstite, I = interstitial glass, K? = kirschsteinite?-feather-shaped laths, α = α-iron, W+F = myrmekitic texture of wüstite and fayalite, N = mechanical twinning.

tures since it is not possible to distinguish between primary and newly formed minerals. Based on the observed textures, however, it can be concluded that Group A is the result of a variation in forging temperature. This group, characterized by the presence of calcium-rich minerals, is interpreted as being the result of a complex smithing process, whereby different temperature regimes were necessary. It is possible that this type of smithing represent the production of complex objects or the finishing step of artifacts. The latter is further supported by the occasionally high Cu-values in this group, indicating brassing of the object in the final stage. The use of fluxes during smithing is typical to avoid oxidation during welding processes or when producing objects with sharp rims (e.g., swords, scissors) (Serneels and Perret 2003).

Group B: Mechanically worked group

The texture of the slag in this group is more homogeneous, indicating a more constant hearth temperature (Bauvais 2007). These temperatures must have been elevated since dendrites are formed. These dendrites are heavily compacted and even form hammer scales, which indicate that the produced objects were

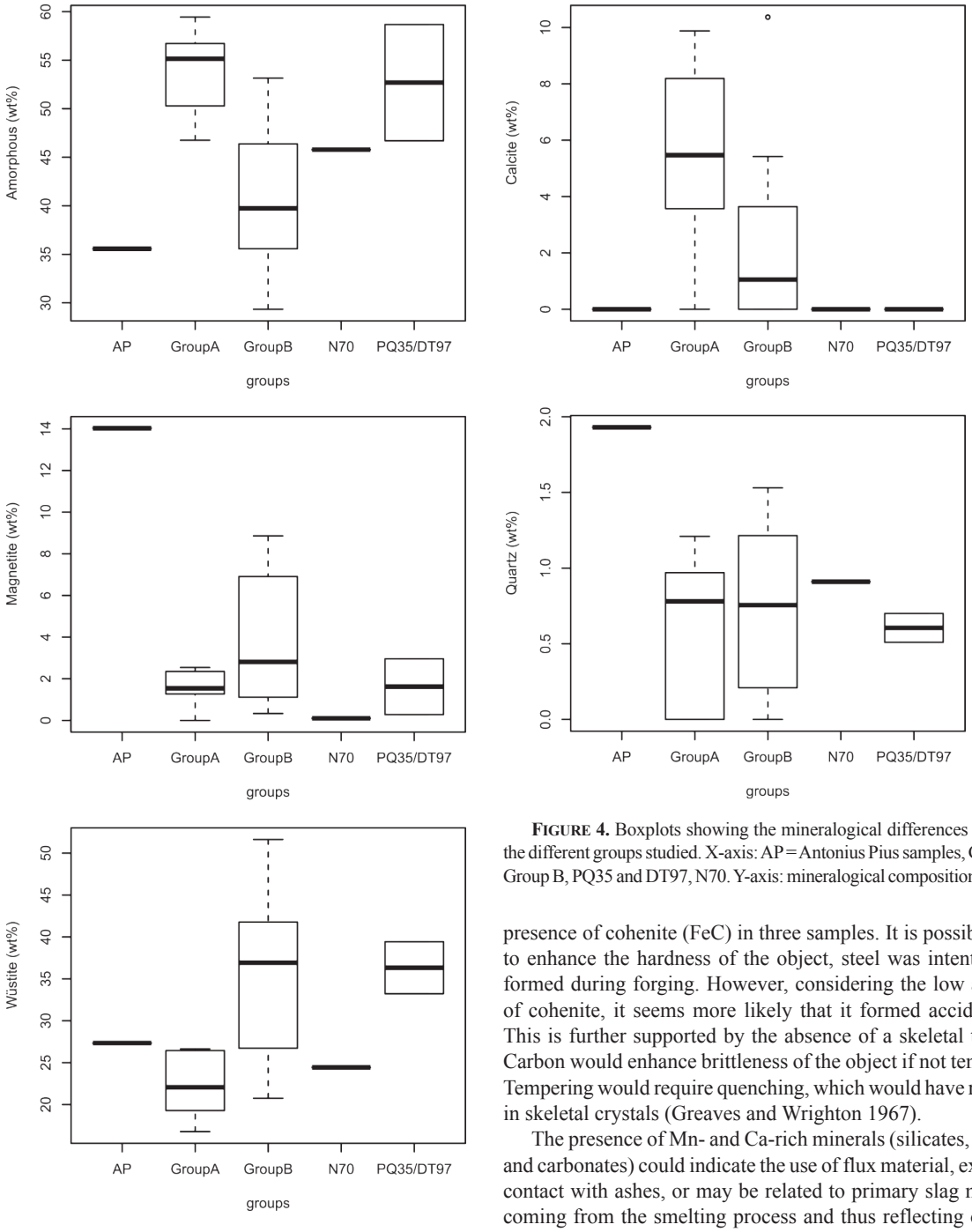

FIGURE 4. Boxplots showing the mineralogical differences between the different groups studied. X-axis: AP = Antonius Pius samples, Group A, Group B, PQ35 and DT97, N70. Y-axis: mineralogical composition in wt%.

mechanically handled after being brought to high temperature (Bauvais 2007). The slag samples have high wüstite (FeO) content, occurring when an outside layer of iron oxide formed after the hot object came in contact with air. Wüstite is stable between 560 and 1370 °C (Kiessling and Lange 1978). In comparison to the temperature-dependent group, more ferrite (α-Fe) is lost. This may be related to the use of a more pure raw product or to the force handling of the object, which would not only expel the outer oxidation layer but some α-Fe as well. Remarkable is the presence of cohenite (FeC) in three samples. It is possible that, to enhance the hardness of the object, steel was intentionally formed during forging. However, considering the low amount of cohenite, it seems more likely that it formed accidentally. This is further supported by the absence of a skeletal texture. Carbon would enhance brittleness of the object if not tempered. Tempering would require quenching, which would have resulted in skeletal crystals (Greaves and Wrighton 1967).

The presence of Mn- and Ca-rich minerals (silicates, oxides, and carbonates) could indicate the use of flux material, extended contact with ashes, or may be related to primary slag material coming from the smelting process and thus reflecting ore and gangue material. The presence of Al-silicates suggests contact of the slag with the hearth lining. Since Al-silicates are more refractory (Bowen and Schairer 1932), this would mean that these minerals are formed in the hottest parts of the hearth (at the air entrance). Based on the variety of minerals, hearth temperature must have been between 560 °C (limit of stability for wüstite; Kiessling and Lange 1978) and 1285 °C (smelting temperature of iron rich gehlenite; Deer et al. 1962). Since more than half of the slag samples contain calcite, temperatures may be further refined to be between 700 and 900 °C (Deer et al. 1962). Refrac-

Table 6. Main mineralogical composition of 21 smithing slag based on quantified XRD Rietveld method (in wt%)

Sample	Amorphous	Akermanite	Calcite	Fayalite	Hematite	Kirschsteinite	Magnetite	Monticellite	Quartz	Wüstite
N311b	50.29	0.00	5.47	0.00	0.63	0.00	1.54	0.00	0.00	19.28
N288	55.15	0.00	9.88	0.69	0.06	0.00	0.00	0.00	0.97	16.77
N396	56.72	4.82	0.00	1.17	0.00	0.00	1.27	0.00	0.78	26.63
N195b	46.75	0.00	8.19	0.27	0.00	0.00	2.54	1.67	0.00	26.44
CS097	59.44	0.78	3.57	0.20	0.61	5.27	2.35	0.00	1.21	22.05
N323	53.15	0.00	2.36	0.67	1.06	0.00	3.26	0.00	0.79	22.14
N269b	47.19	4.01	5.42	0.65	0.00	0.00	2.36	0.00	0.00	34.12
CS027	36.40	0.00	0.52	0.00	0.00	23.00	0.33	3.95	0.00	28.71
CS022	34.74	0.00	0.00	26.69	0.47	0.00	0.52	0.05	0.72	20.75
CS264	42.27	0.00	0.00	0.00	0.00	0.00	1.21	0.00	1.16	50.86
B263	40.07	0.00	0.00	0.61	0.00	3.89	4.51	1.74	0.42	40.37
91F	39.40	0.00	10.37	0.81	0.99	0.00	2.14	0.00	1.53	29.62
L475	29.34	0.00	1.59	0.53	0.00	0.00	7.57	0.70	1.37	43.16
LW033	45.57	0.00	2.25	0.00	0.49	0.00	1.01	0.00	0.68	40.23
LE600b	52.00	0.00	0.00	0.00	0.00	0.00	8.86	0.00	1.27	24.74
UAN232	33.95	0.00	0.00	0.63	0.87	0.00	6.25	0.00	0.90	51.63
DA2177	38.28	0.00	4.92	0.00	0.00	0.00	7.84	0.00	0.00	39.74
AP181C	35.57	0.00	0.00	0.00	0.62	0.00	14.03	0.00	1.93	27.33
N70E	45.78	0.00	0.00	0.00	0.00	21.35	0.10	0.00	0.91	24.43
PQ35B	58.68	0.00	0.00	1.06	0.00	0.00	0.28	5.59	0.70	33.22
DT097	46.70	0.00	0.00	0.00	0.51	5.19	2.96	0.00	0.51	39.42

tory minerals can be primary slag of the bloom or bar, or formed in the forging hearth at the air entrance.

There are two hypotheses regarding the formation of these slag samples. It is possible that this group of slag represents bar smithing. The compaction of the bloom to a bar, demand frequent, forced hammering (Crew 1991). However, one would expect more slag material (silicates) and less iron oxides to be expelled when smithing bloom to bar. It is more likely that a simple object was smithed, e.g., hammers, rods, or nail heading tools (Manning 1976; Sim 2012). The smith must have repeatedly heated and hammer the billet. No finishing work (except scraping of the iron oxides) was necessary (Sim 2012). This type of work would result in the homogeneous textures described above.

Other samples

PQ35 and DT97. Based on the observed textures it seems that a blacksmith combined high-temperature forging (skeletal shape wüstite) with force mechanical handling (hammer scales). There is only limited loss of ferrite during this process. Mineralogical, there is less variation than in groups A and B. The samples have a high-amorphous phase similar to the temperature-dependent group and have relatively high amounts of wüstite like the mechanical group. In sample PQ35 monticellite ($CaMgSiO_4$) is present in higher abundances compared to the other groups. Monticellite is stable below 890 °C. Above this temperature it will react with CO_2 to form akermanite and forsterite (Deer et al. 1982). Sample DT97 shows the presence of kirschsteinite ($CaFeSiO_4$). Kirschsteinite shows unlimited solid solution with fayalite (Markl et al. 2001). The temperature stability of kirschsteinite at low pressure is between 850 and 930 °C.

Elevated K_2O, MgO, and Na_2O contents observed in the two samples, are interpreted to be associated with fuel ashes (Charlton et al. 2013). These two samples show a more varied smithing activity than group A and B. The mineralogical composition and observed textures are consistent with heating and mechanical working at elevated temperatures. Since no stratification is recognized, the observed textural patches do not represent different phases in the smithing of the object. It is possible that these slag samples represent a phase toward the end of the smithing. Mainly iron oxides are removed from the object. High temperatures are required for this object resulting in the high content of amorphous phase and skeletal texture. Another possibility is that the interaction with ashes altered the otherwise mechanically worked samples. The MgO, K_2O, and Na_2O in the ashes will act as a flux.

Antonius Pius samples. The Antonius Pius samples show a different texture from the other groups. Next to hammer scale textures, a myrmekitic texture is observed resembling pearlite. However, the latter is only seen in steel. Chemical and mineralogical composition support the idea that the observed texture is in fact an eutectic texture of wüstite and fayalite (Fe_2SiO_4) formed at temperatures below 1205 °C (Crook 1939). This would imply that the smith was working at elevated temperatures compared to the other groups or that it is a primary mineral from the smelting process. Compared with the other groups, these samples also have the highest quartz content. Free quartz implies addition of a flux or a protective agent against oxidation (Crew 1991; Sherby and Wadsworth 2001; Serneels and Perret 2003; Bauvais 2007). Also magnetite is high in comparison to the other groups. If the magnetite was a relic of the ore used, one would expect to see euhedral crystals. This is not the case, implying that magnetite was formed during oxidation of iron at temperatures above 580 °C in the hearth (Bowles et al. 2011). Remarkable for these smithing slag samples are the low content in amorphous phases, suggesting slow cooling. It is possible that the smith worked at high temperatures at the start of the forging, which would explain the eutectic texture. Since quartz is present in its α-form and not converted to cristobalite, silica was added later in the process, e.g., for welding. It is however also possible that the eutectic is a primary structure, which implies that these samples could be classified in the mechanically worked group.

N70E. The dominant feather-like laths of this sample indicate high-temperature processes or rapid cooling (Deer et al. 1982; Serneels 1993). The crystal shapes of wüstite support this idea. Little iron oxide is observed, which implies low oxidation. Remarkably high α-iron content is observed.

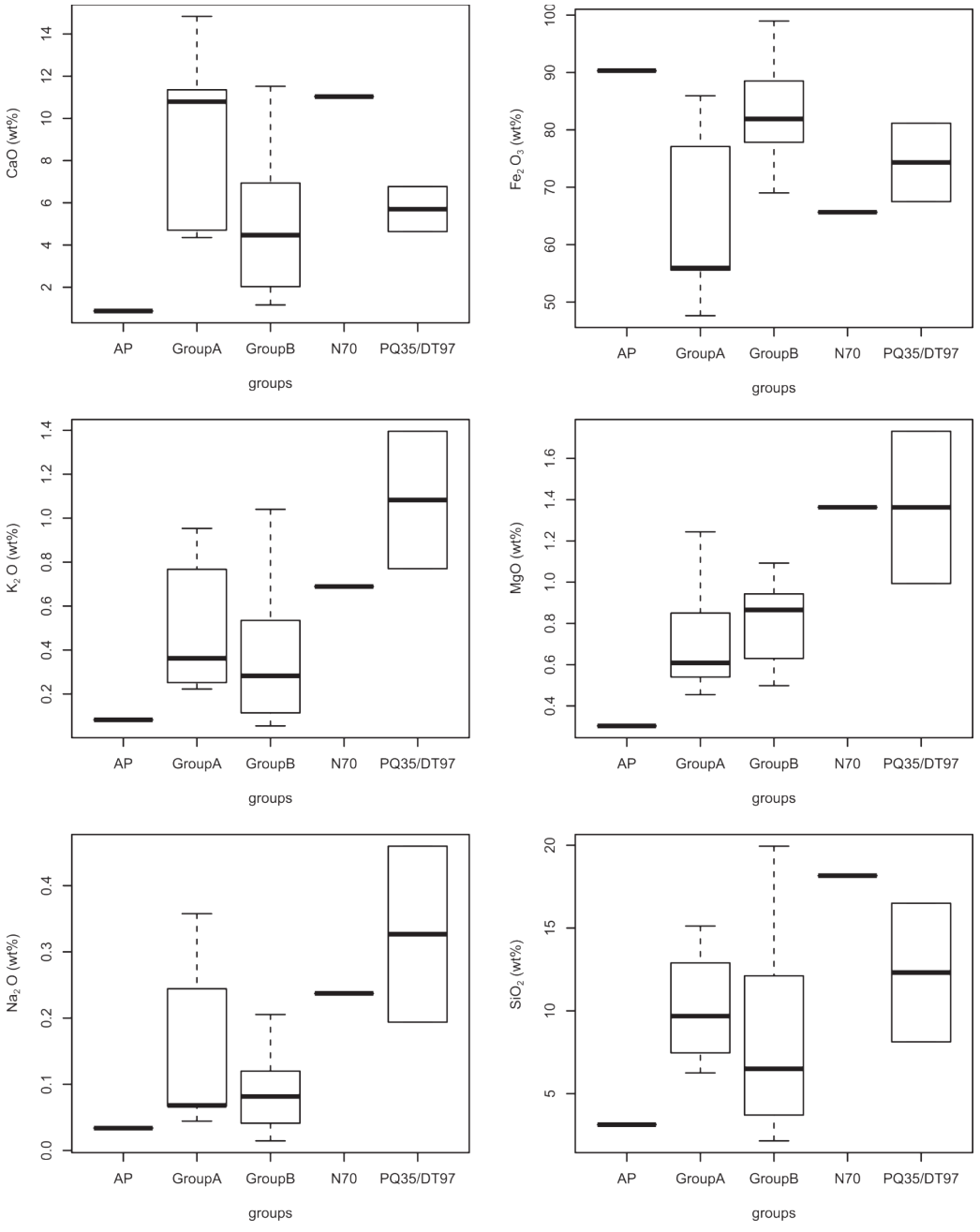

Figure 5. Boxplots showing the chemical differences between the different groups studied. X-axis: AP = Antonius Pius samples, Group A, Group B, PQ35 and DT97, N70. Y-axis: chemical composition in wt%.

Since kirschsteinite content is dominant according to the quantitative XRD results, it is assumed that the feather-shaped laths are kirschsteinite with minor forsterite (Mg_2SiO_4). First, kirschsteinite may be formed from the reaction of wollastonite and magnetite at 850–930 °C (Markl et al. 2001). This would mean that in the original bar the latter minerals were present, but this cannot be confirmed. No exsolution textures are observed in optical microscopy. Second, kirschsteinite could also be the result of using flux material during smelting or smithing. It is however not possible to assign kirschsteinite to one or the other. The observed twinning in the iron oxides is identified as Neumann bands and is regarded as a type of mechanical twinning. They originate from explosive impact at room temperature (Greaves and Wrighton 1967). The shape of the twins, which are more tapered, confirm that they are deformation twins (Passchier and Trouw 2005). This sample possibly represents the starting phase of smithing: the bar is left in the hearth so that the slag liquates from the bloom/bar (Crew

1991). When the bar however is left too long, unconsolidated α-iron is lost (Crew 1991). After this working phase, the object will be compacted by hammering (Crew 1991), which would explain the observed Neumann bands.

Change in techniques through time?

Two main smithing techniques can be recognized in the smithing slag of Sagalassos. The first one shows a large variation in applied temperature. High-calcite content indicates the use of local limestone as flux or to facilitate the welding process. This smithing technique likely indicates the production of complex artifacts that needed welding or a cutting edge (scissors, knife, sword). The second technique applies high-temperature conditions with little variation. The main activity consists of heating and hammering. This technique is applied for forging simple bulk material, such as hammers. Both smithing techniques are used contemporaneously. There does not seem to be a technological change through time that could be related to potential economic (specialization) or political (conflict) changes. The mechanical group is dominant through the entire Roman period (Table 5), indicating that the main iron production in Sagalassos is focused on the production of simple tools. The current study demonstrates the importance of smithing slag in reconstructing the technological evolution of iron production at a particular site.

TABLE 7. Chemical data set of 21 smithing slag determined by ICP-OES (oxides in wt% trace elements in parts per million)

Sample	Al_2O_3	BaO	CaO	Fe_2O_3	K_2O	MgO	MnO	Na_2O	P_2O_5	SiO_2	TiO_2	Cu
N396	3.76	0.06	14.83	55.54	0.95	1.24	0.18	0.36	0.52	15.12	0.15	564.07
NK195b	1.20	0.01	4.36	85.93	0.25	0.45	0.04	0.04	0.62	6.25	0.03	246.05
N311b	1.75	0.03	4.70	47.62	0.22	0.54	0.05	0.07	0.39	7.47	0.03	239.62
N288	3.25	0.05	11.35	55.92	0.77	0.85	0.17	0.24	0.57	12.90	0.10	364.03
CS097	1.58	0.01	10.79	77.09	0.36	0.61	0.34	0.07	0.54	9.68	0.03	178.32
N323	1.15	0.02	2.43	83.21	0.09	0.88	0.24	0.01	0.54	6.52	0.05	113.38
N269b	1.16	0.01	6.55	80.61	0.13	0.85	0.20	0.04	0.30	5.96	0.05	673.62
CS264	1.37	0.02	3.07	87.84	0.42	0.95	0.29	0.09	0.35	4.51	0.03	777.24
CS022	2.46	0.06	5.87	69.54	0.60	0.86	1.48	0.12	0.38	19.94	0.08	92.47
CS027	2.64	0.03	11.52	69.02	1.04	1.09	0.48	0.21	0.88	15.89	0.12	391.59
LW033	0.97	0.01	1.25	89.20	0.13	0.52	0.33	0.04	0.34	2.91	0.01	89.48
L475	2.10	0.02	7.20	78.83	1.02	0.97	0.55	0.12	0.41	14.15	0.11	223.78
LE600b	0.72	0.01	1.62	98.97	0.10	0.88	0.26	0.07	0.31	2.15	0.00	87.39
UAN232	0.91	0.01	1.16	97.08	0.05	0.50	0.26	0.03	0.30	2.63	NA	90.36
DA2177	2.52	0.08	6.68	79.23	0.24	0.93	0.17	0.12	0.24	10.09	0.09	132.39
B263	1.27	0.01	2.68	85.42	0.47	0.68	0.15	0.07	0.21	6.49	0.03	123.21
91F	1.77	0.05	8.51	76.85	0.33	0.58	0.27	0.11	0.41	9.12	0.04	165.96
AP181c	0.87	0.01	0.88	90.32	0.08	0.30	0.01	0.03	0.24	3.13	0.01	112.44
N70e	3.83	0.02	11.03	65.65	0.69	1.36	0.20	0.24	0.38	18.16	0.18	110.89
DT097	2.24	0.04	4.63	81.16	0.77	0.99	0.75	0.19	0.36	8.13	0.08	240.86
PQ035b	4.50	0.04	6.77	67.49	1.40	1.73	0.21	0.46	0.32	16.50	0.22	104.61

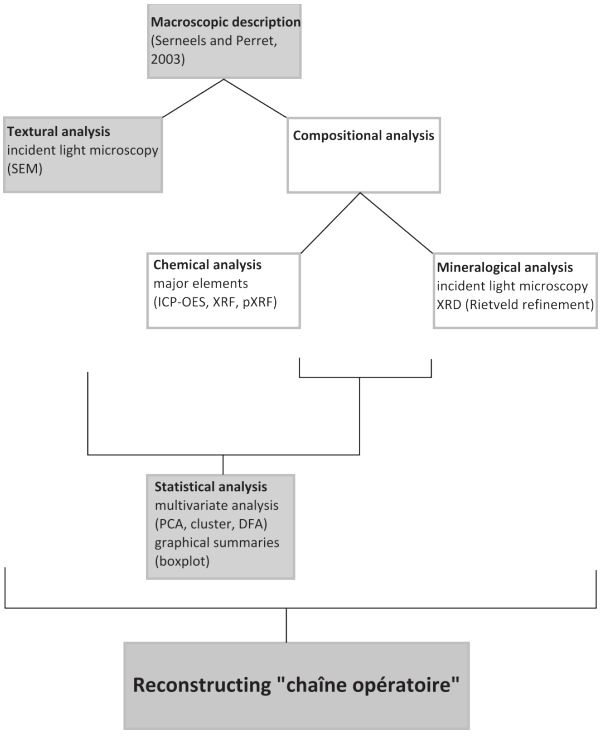

FIGURE 6. Workflow chart for the analysis and interpretation of smithing slag. Steps in gray are the necessary steps in the procedure. Compositional analysis are recommended since they complement the textural analysis.

IMPLICATIONS

Most archaeometallurgical studies focus mainly on smelting slag using geochemical analysis to reconstruct the operational chain of the iron production of a particular site. Smithing slag are often excluded from further study due to their large chemical variability. This paper, however, shows that by focusing on microscopic textural analysis, supported by compositional data, it is possible to reconstruct ancient smithing techniques, an indispensable factor in the production chain. Although this article in first instance contributes to the field of archaeology, archaeometry, and archaeometallurgy, it is also of interest to research on recent metallurgical waste. A general methodological strategy when working with (iron) slag is presented (Fig. 6). A solution to overcome recurring problems in refining XRD implementation code when working with iron (hydro) oxides and solid solution minerals is suggested. Additionally, it offers a description of mineralogical textures in slag that are the result of human intervention and in this way contributes to material science in general.

ACKNOWLEDGMENTS

This research was supported by the Belgian Programme on Interuniversity Poles of Attraction (IAP 07/09 CORES). All analytical and interdisciplinary research within the framework of the Sagalassos Project is carried out within the framework of the "Centre for Archaeological Sciences" of the University of Leuven. We want to thank the "Sagalassos Archaeological Research Project" led by Jeroen Poblome for the support during the field campaigns. We are very grateful to Steven Luypaers for his help with the sample preparations, to Elvira Vasillieva for the assistance with the chemical analysis, to Herman Nijs for making the polished sections and to Rieko Adriaens for the help with the XRD interpretations. Special thanks go to blacksmith Arne Maerschalck to introduce us in his world. We are also grateful to the editor and the two anonymous reviewers for their feedback to improve this manuscript.

REFERENCES CITED

Bachmann, H.-G. (1982) The identification of slags from archaeological sites. Institute of Archaeology, University College London.

Baerlocher, C. (1986) Zeolite structure refinements using powder data. Zeolites, 6, 325–333.

Bauvais, S. (2007) Evolution de l'organisation des activités de forge dans le nord du Bassin Parisien au second Age du Fer, 606 p. Unpublished Ph.D. thesis, Université de technologie de Belfort-montbeliard, Université de Franche-Comte.

Berranger, M., and Fluzin, P. (2007) Organisation de la chaîne opératoire en métallurgie du fer aux deuxièm-premier siècle av.J.-C., sur l'oppidum d'Entremont (Aix-en-Provence, Bouches-du-Rhône): la circulation du métal. ArchéoSciences, 31, 7–22.

Bowen, N.L., and Schairer, J.F. (1932) The system FeO-SiO_4. American Journal, 24, 177–213.

Bowles, J.F.W., Howie, R.A., Vaughan, D.J., and Zussman, J. (2011) Rock form-

ing minerals V5A: Non-silicates (oxides, hydroxides and sulphides), 920 p. Geological Society London.
Brems, D. (2011) Mineralogy and geochemistry of Mediterranean sand deposits as a raw material for Roman natron glass production, 134 p. Unpublished Ph.D. thesis, KU Leuven.
Charlton, M., Crew, P., Rerhen, T., and Shennan, S. (2013) Measuring variation in iron smelting slags: An emperical evaluation of group-identification procedures. In J. Humpris and T. Rehren, Eds., The World of Iron, p. 421–430. Archetype, London.
Cleere, H. (1971) Iron making in a Roman furnace. Britannia, 2, 203–217.
——— (1976) Some operating parameters for Roman ironworks. Bulletin of the Institute of Archaeology, 13, 233–246.
Crew, P. (1991) The experimental production of bar iron. Journal of the Historical Metallurgy Society, 25, 21–36.
——— (1996) Bloom refining and smithing slags and other residues. In Archaeology datasheet, p. 6. The Historical Metallurgy Society, Gateshead, U.K.
Crook, W.J. (1939) The series iron oxides-silica. Journal of the American Ceramic Society, 22, 322–334.
Deer, W.A., Howie, R.A., and Zussman, J. (1962) Rock forming minerals V1: Ortho- and ring silicates, 331 p. Longman, London.
——— (1978) Rock Forming Minerals V2A: Single chain silicates, 667 p. Longman, London.
——— (1982) Rock-Forming Minerals V1A: Orthosilicates, 919 p. Longman, London.
——— (2013) An introduction to rock forming minerals, 498 p. Berforts Information Press, London.
Degryse, P., Poblome, J., Donners, K., Deckers, J., and Waelkens, M. (2003a) Geoarchaeological investigations of the potters quarter at Sagalassos, southwest Turkey. Geoarchaeology, 18, 255–281.
Degryse, P., Muchez, P., Naud, J., and Waelkens, M. (2003b) Iron production at the Roman to Byzantine city of Sagalassos: an archaeometrical case study. In Archaeometallurgy in Europe, 133–142. Associazione Italiana di Metallurgia, Milaan, Italy.
Degryse, P., Schneider, J., Kellens, N., Waelkens, M., and Muchez, Ph. (2007) Tracing the resources of iron working at ancient Sagalassos (south-west Turkey): A combined lead and strontium isotope study on iron artefacts and ores. Archaeometry, 49, 75–86.
Degryse, P., Schneider, J., and Muchez, P. (2009) Combined Pb-Sr isotopic analysis in provenancing late Roman iron raw materials in the territory of Sagalassos (SW Turkey). Archaeological and Anthropological Sciences, 155–159.
Donaldson, C.H. (1976) An experimental investigation of olivine morphology. Contributions to Mineralogy and Petrology, 57, 187–213.
Greaves, R.H., and Wrighton, H. (1967) Practical microscopical metallography, 221 p. Chapman and Hall, London.
Kellens, N., Degryse, P., Martens, F., and Waelkens, M. (2003) Iron production activities and products at Roman to Early-Byzantine Sagalassos (SW Turkey). In Archaeometallurgy in Europe, 1382–1893. Associazione Italiana di Metallurgia, Milaan, Italy.
Kiessling, R., and Lange, N. (1978) Non-Metallic Inclusions in Steel, 465 p. Iron and Steel Institute, the Metals Society, London.
Klein, C., and Dutrow, B. (2008) The Manual of Mineral science, 675 p. Wiley, New York.
Le Carlier, C., Leroy, M., and Merluzzo, P. (2007) L'apport de l'analyse morphologique, microscopique et chimique des scories en forme de culot à la restitution des activités de forge. ArcheoSciences, 23–35.
Martens, F. (2005) The archaeological urban survey of Sagalassos (South-west Turkey): The possibilities and limitations of surveying a "non-typical" Classical site. Oxford Journal of Archaeology, 24, 229–254.
Manning, W.H. (1976) Blacksmithing. In D. Strong and D. Brown, Eds., Roman Crafts, 256 p. Duckworth, London.
Markl, G., Marks, M., and Wirth, R. (2001) The influence of T, $aSiO_2$, and fO_2 on exsolution textures in Fe-Mg olivine: An example from augite syenites of the Ilimaussaq Intrusion, South Greenland. American Mineralogist, 86, 36–46.
Mertens, G. (2009) Characterisation of historical mortars and mineralogical study of the physico-chemcial reactions on the pozzolan-lime binder interface, 266 p. Unpublished Ph.D. thesis, Leuven, Belgium.
Passchier, C.W., and Trouw, R.A.J. (2005) Microtectonics, 366 p. Springer, Berlin.
Poblome, J. (1999) Sagalassos Red Slip Ware: Typology and chronology, 500 p. Brepols, Turnhout, Belgium.
Rehren, T., and Pernicka, E. (2008) Coins, artefacts and isotopes–Archaeometallurgy and Archaeometry. Archaeometry, 50, 232–248.
Rietveld, H.M. (1967) Line profiles of neutron powder-diffraction peaks for structure refinement. Acta Crystallographica, 22, 151–152.
Serneels, V. (1993) Archéométrie des scories de fer. Recherches sur la sidérurgie ancienne en Suisse occidentale, p. 232. Cahiers d'archéologie Romande N°61, collection creée par Colin Martin.
Serneels, V., and Perret, S. (2003) Quantification of smithing activities based on the investigation of slag and other material remains. In Archaeometallurgy in Europe-Proceedings of the International Conference, 469–478. Associazione Italiana di Metallurgia, Milaan, Italy.
Sherby, O.D., and Wadsworth, J. (2001) Ancient blacksmiths, the Iron Age, Damascus steels, and modern metallurgy. Journal of Materials Processing Technology, 117, 347–353.
Sim, D. (1998) Beyond the Bloom: bloom refining and iron artefact production in the Roman world, 155 p. Archaeopress, Oxford.
——— (2012) The Roman Iron Industry in Britain, 174 p. The History Press, Brimscombe, Gloustershire, U.K.
Srodon, J., Drits, V.A., McCarty, D.K., Hsieh, J.C.C., and Eberl, D.D. (2001) Quantitative X-ray diffraction analysis of clay bearing rocks from random preparations. Clays and Clay Minerals, 49, 514–528.
Vyncke, K. (2013) Düzen Tepe: The potential of contextual analysis and functional space analysis by means of an interdisciplinary archaeological and archaeometric research at a Classical-Hellenistic site, 542 p. Unpublished Ph.D. thesis, Katholieke Universiteit, Leuven, Belgium.
Waelkens, M. (2002) Romanization in the East. A case study: Sagalassos and Pisidia (SW Turkey). Istanbuler Mitteilungen, 52, 311–368.
Young, T. (2012) Iron: Hand blacksmithing. In Archaeology datasheet p. 303. The Historical Metallurgy Society, Gateshead, U.K.

Manuscript received April 24, 2015
Manuscript accepted October 18, 2015
Manuscript handled by Callum Hetherington